

Citation	J. Quesada, and G. AlRegib, "Scale-Aware Self-Supervised Learning for Segmentation of Small and Sparse Structures", accepted at 2026 IEEE International Conference on Acoustics, Speech, and Signal Processing (ICASSP)
Review	Date of acceptance: 17 January 2026
Code & Data	https://github.com/olivesgatech/SASSL
Bib	@ARTICLE{Quesada2026Scale, author={J. Quesada and G. AlRegib}, journal={IEEE International Conference on Acoustics, Speech, and Signal Processing}, title={Scale-Aware Self-Supervised Learning for Segmentation of Small and Sparse Structures}, year={2026},}
Copyright	©Creative Commons Attribution CCBY 4.0
Contact	{jpacora3, alregib}@gatech.edu https://alregib.ece.gatech.edu/
Corresponding author	alregib@gatech.edu

SCALE-AWARE SELF-SUPERVISED LEARNING FOR SEGMENTATION OF SMALL AND SPARSE STRUCTURES

Jorge Quesada and Ghassan AlRegib

OLIVES at the Georgia Institute of Technology

ABSTRACT

Self-supervised learning (SSL) has emerged as a powerful strategy for representation learning under limited annotation regimes, yet its effectiveness remains highly sensitive to many factors, especially the nature of the target task. In segmentation, existing pipelines are typically tuned to large, homogeneous regions, but their performance drops when objects are small, sparse, or locally irregular. In this work, we propose a scale-aware SSL adaptation that integrates small-window cropping into the augmentation pipeline, zooming in on fine-scale structures during pretraining. We evaluate this approach across two domains with markedly different data modalities: seismic imaging, where the goal is to segment sparse faults, and neuroimaging, where the task is to delineate small cellular structures. In both settings, our method yields consistent improvements over standard and state-of-the-art baselines under label constraints, improving accuracy by up to 13% for fault segmentation and 5% for cell delineation. In contrast, large-scale features such as seismic facies or tissue regions see little benefit, underscoring that the value of SSL depends critically on the scale of the target objects. Our findings highlight the need to align SSL design with object size and sparsity, offering a general principle for building more effective representation learning pipelines across scientific imaging domains.

Index Terms— Self-supervised learning, Semantic segmentation, Seismic interpretation, Neuroimaging

1. INTRODUCTION

Self-supervised learning (SSL) has become a cornerstone of modern representation learning, enabling models to leverage large unlabeled datasets through pretext tasks rather than costly manual annotations [1–3]. Its effectiveness has not only driven advances across vision [1, 4], medical imaging [5, 6], and remote sensing [7, 8], but has also laid the foundation for the rise of transformer architectures [9–11], whose pretraining paradigms are inherently self-supervised [12, 13]. Despite these successes, most existing SSL pipelines implicitly assume that learned features should capture broad, homogeneous patterns. This design choice aligns well with tasks such as classification or object recognition, but its suitability for tasks dominated by small or sparse structures remains unclear.

Segmentation tasks provide a natural testbed for this question. In many domains, targets vary drastically in their spatial scale: large and continuous regions such as organs [14] or geological facies [15] contrast sharply with small and rare structures such as neurons, blood vessels [5], or seismic faults [16]. Standard SSL approaches often underperform on the latter, as pretraining objectives dominated by large contextual patterns fail to emphasize the fine-scale cues required for accurate segmentation. Figure 1 illustrates this mismatch

using segmentation tasks from geophysics [16] and neuroscience [5]: the same SSL pipeline that yields useful representations for large structures struggles to capture narrow or localized ones, either by merging them into a single large object losing granularity (seismic case), or by capturing only the most salient ones (neuroscience case).

In this work, we argue that the effectiveness of SSL in segmentation depends critically on the scale and sparsity of the target objects. To address this, we propose a simple yet effective scale-aware strategy that embeds small-window cropping directly into the augmentation process, forcing encoders to “zoom in” on localized features during pretraining. This modification biases representations toward fine-grained structures without requiring architectural changes or additional supervision. We validate this approach across two distinct scientific imaging domains: (i) seismic imaging, where faults appear as narrow, discontinuous anomalies within large volumes, and (ii) neuroimaging, where cells and other microscopic structures are small and spatially sparse relative to the surrounding tissue. Our experiments demonstrate that scale-aware SSL provides consistent improvements in both settings under limited labels, yielding up to 13% accuracy gains for fault segmentation and 5% for blood cell and vessel delineation. By contrast, tasks involving larger-scale features (such as seismic facies or axon regions) show little benefit, underscoring the importance of tailoring SSL strategies to the intrinsic properties of the segmentation target.

2. RELATED WORK

Segmentation tasks vary widely in terms of the spatial scale and density of the target structures. Deep learning has achieved strong results for segmenting large to mid-size homogeneous regions such as organs or geological facies [15, 17]. In contrast, small or sparse structures continue to be more challenging because of their limited spatial footprint, sparsity, and irregular geometry [18, 19]. This gap suggests that scale strongly influences representation quality for downstream segmentation tasks.

SSL has made substantial progress with global contrastive methods (SimCLR [1], MoCo [2]), non-contrastive ones (BYOL [20], SimSiam [4]), among others for a wide variety of downstream tasks. However, these methods typically assume (or are optimized for) features that capture broad semantic structure. Thus many SSL pipelines achieve good transfer performance on downstream dense prediction tasks when the objects of interest have well-defined and reasonably large spatial extent, as we showcase in Figure 1.

Recent works, however, begin to challenge this assumption. [21] observes that methods that include multiscale views, patch-based tasks, or dense pixel/patch clustering often behave better when the downstream task involves fine-grained or spatially localized structures. [22] learns both global and local features to target segmentation tasks, [18] enforces inter-scale consistency, and [19] addresses

This work is supported by the ML4Seismic Industry Partners at Georgia Tech

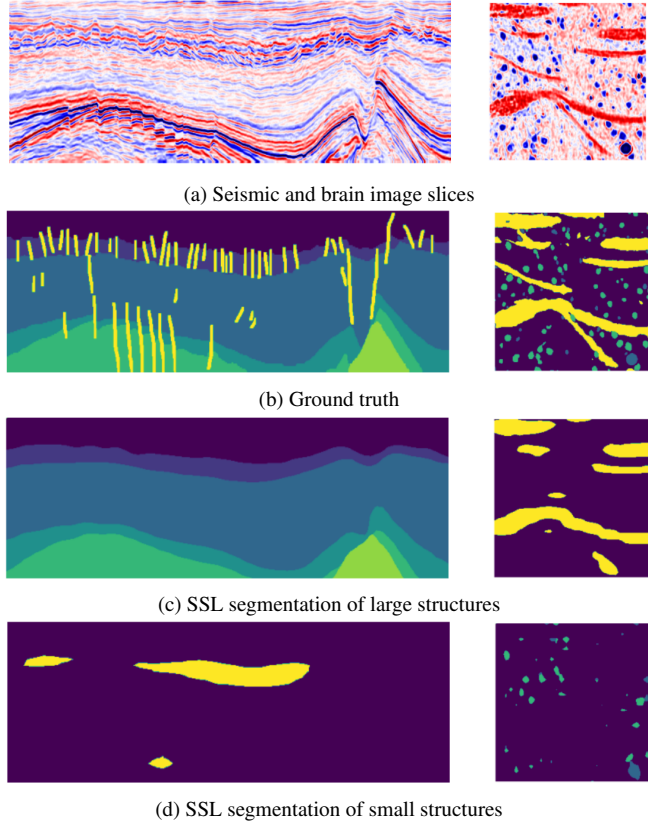


Fig. 1: Differences in SSL segmentation depend on the nature of the target. Left: Seismic segmentation task with geological facies (large) and seismic faults (small). Right: Neuroimaging segmentation task from a mouse brain cutout, with axons (large) and cell bodies and vessels (small).

inconsistencies in non-salient regions. These methods highlight the importance of balancing local and global cues during SSL pretraining.

While prior work recognizes the value of multi-scale or patch-level cues, few studies systematically analyze the impact of object scale and sparsity on SSL performance across domains. Our work addresses this gap by explicitly embedding small-window cropping into SSL pretraining and validating its effect on small, sparse targets in both seismic and neuroimaging data.

3. METHODOLOGY

3.1. Self-Supervised Pretraining

We adopt a general SSL framework where an encoder f_θ learns representations from unlabeled images by enforcing consistency between multiple augmented views of the same sample. Given an input image $x \in \mathbb{R}^{H \times W}$, two stochastic augmentations $t_1, t_2 \sim \mathcal{T}$ produce correlated views $x_1 = t_1(x)$, $x_2 = t_2(x)$. Each view is passed through the encoder and optionally a projection head g_ϕ , yielding embeddings $z_i = g_\phi(f_\theta(x_i))$. Different SSL algorithms are instantiated differently:

- **Contrastive approaches** (e.g., SimCLR, MoCo) maximize similarity between embeddings of positive pairs while con-

trasting them against negatives.

- **Non-contrastive approaches** (e.g., BYOL, SimSiam) align embeddings without explicit negatives, using asymmetry or stop-gradient mechanisms to avoid collapse.
- **Regularization-based approaches** (e.g., VICReg [23]) enforce view alignment through an ℓ_2 loss while explicitly preventing collapse by adding variance and covariance regularizers on the embedding distribution.

Formally, the SSL objective can be expressed as:

$$\mathcal{L}_{SSL} = \sum_{i=1}^N \ell(z_{i1}, z_{i2}; \{z_j\}_{j \neq i}), \quad (1)$$

where ℓ denotes a contrastive, predictive, or clustering-based loss depending on the chosen SSL method, z_{i1}, z_{i2} are the positive view pairs extracted from sample x_i , and $\{z_j\}_{j \neq i}$ is the set of negative contrastive views.

3.1.1. Scale-Aware View Sampling

Our key contribution is to modify the augmentation process \mathcal{T} to include *scale-aware cropping*, ensuring that pretraining emphasizes fine-grained patterns. Specifically, instead of restricting views to global or large crops, we explicitly sample *small spatial windows* of fixed size $h \times w$ from the input x :

$$t(x) = a(c(x)), \quad (2)$$

where $c : \mathbb{R}^{H \times W} \rightarrow \mathbb{R}^{h \times w}$ is a cropping function and $a \in \mathcal{A}$ is a set of standard augmentations (flips, intensity jitter, affine transforms).

Two strategies for sampling crop centers are considered:

1. **Random cropping:** patch centers are sampled uniformly from the image.
2. **Proximity-constrained cropping:** given a first crop center (u_1, v_1) , a second crop is sampled within distance δ , i.e.

$$\|(u_2, v_2) - (u_1, v_1)\|_2 < \delta, \quad (3)$$

encouraging overlap and spatial coherence.

Embedding this small-window sampling directly into SSL forces the encoder to attend to localized structures that may otherwise be underrepresented in large-scale views. This design is agnostic to the underlying SSL objective and can be plugged into contrastive, non-contrastive, or clustering-based frameworks.

3.2. Downstream Segmentation

After pretraining, the encoder f_θ is integrated into a supervised segmentation network for fault delineation. We adopt a standard encoder-decoder architecture, where the pretrained encoder initializes the feature extraction layers and a randomly initialized decoder is appended to produce voxel-wise segmentation maps. During this stage, training is performed on a small labeled subset of the seismic dataset, consistent with the label-constrained regime.

Formally, given a labeled image $x \in \mathbb{R}^{H \times W}$ and its corresponding binary fault mask $Y \in \{0, 1\}^{H \times W}$, we extract training samples as patches of the same spatial size $(h \times w)$ used during SSL pretraining $x_{(u,v)}, y_{(u,v)}$, where (u, v) denotes the patch center coordinates. Each patch is passed through the encoder-decoder to yield a predicted mask

$$\hat{y}_{(u,v)} = \sigma(F_\psi(f_\theta(x_{(u,v)}))),$$

with F_ψ denoting the decoder and σ the sigmoid activation. Training minimizes the Dice loss between $\hat{y}_{(u,v)}$ and $y_{(u,v)}$.

At inference time, a full image is segmented by sliding a window of size $h \times w$ with stride $s < h$. Predictions from overlapping patches are averaged to produce the stitched full-slice segmentation. This reconstruction ensures seamless predictions across patch boundaries.

Performance is evaluated by comparing stitched predictions \hat{Y} against ground-truth masks Y using standard segmentation metrics. This patch-based training and inference strategy ensures compatibility with the encoder’s pretraining resolution while simultaneously retaining the original scale of the image.

4. RESULTS

4.1. Experimental Setup

We evaluate our approach on two distinct domains that naturally lend themselves to segmentation of small or sparse structures:

- **Seismic fault segmentation**, where targets correspond to thin and discontinuous linear faults embedded in noisy seismic volumes. We use the CRACKS [16] and Thebe [24] datasets for this purpose.
- **Segmentation of cellular structures in neuroimaging data**, where targets are small, compact objects relative to surrounding tissue. We use the MTNeuro dataset [5] for this domain.

For each dataset, the full set of training images are available for self-supervised pretraining, while only a small fraction of labeled samples (10% unless otherwise noted) is used for downstream segmentation. This reflects the label-constrained regime common in different domains of scientific imaging, where acquiring labels is a costly and time-consuming endeavor.

We evaluate three representative SSL methods: SimCLR, BYOL, and VICReg, covering multiple SSL paradigms. All models share a ResNet-18 backbone, trained for 100 epochs with batch size 128 and the LARS optimizer. Scale-aware cropping is embedded into the augmentation pipeline, with patches of size $L/2$, $L/4$, and $L/8$ sampled per image (L is the smallest image dimension for each dataset). Both random and proximity-constrained cropping strategies are tested, combined with standard augmentations (flips, intensity jitter, affine transforms). Results are reported as averages across the three SSL methods to reduce method-specific variance.

We compare against fully supervised models trained directly on the limited labeled data, and SSL baselines including vanilla SimCLR trained with global scope only (no scale-aware sampling) and VICRegL [22], a VICReg adaptation targeted towards segmentation by focusing on global and local features. For downstream segmentation, pretrained encoders are coupled with a DeepLabV3 decoder and fine-tuned using Dice loss. Inference is performed with overlapping sliding windows. Performance is evaluated with Dice coefficient (region overlap) and Hausdorff distance (structural and boundary alignment).

To complement our experiments, we also leverage the fact that both the CRACKS and MTNeuro datasets provide large-structure segmentation targets. On CRACKS, we evaluate facies segmentation, where lithostratigraphic units occupy a much larger portion of the seismic volume than faults. On MTNeuro, we evaluate axon segmentation, targeting neural structures substantially larger than the cells and vessels used in our main setup. These additional tasks allow us to assess how the *same SSL representations* transfer to segmentation targets of different scales within the same data.

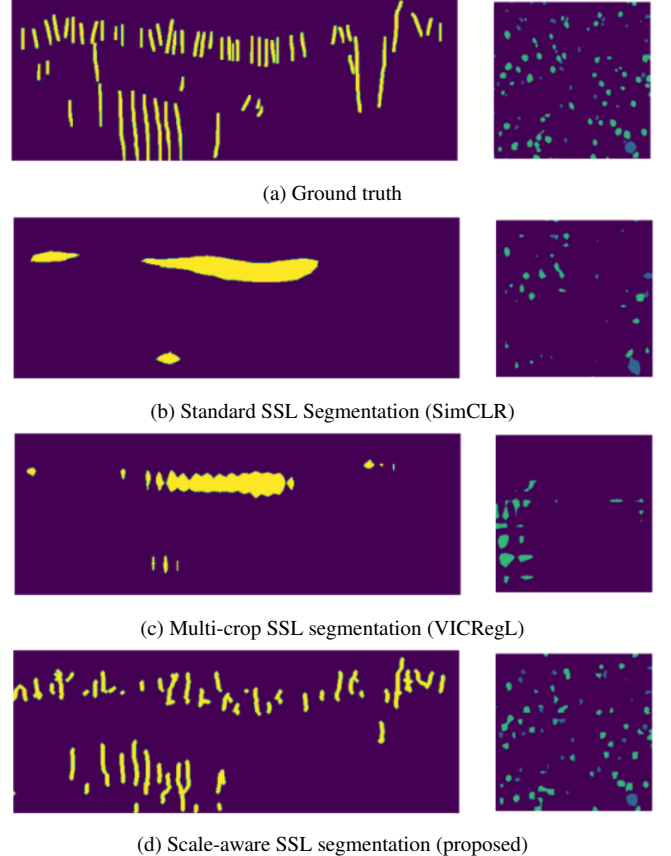


Fig. 2: Qualitative segmentation results for CRACKS (left) and MTNeuro (right).

All SSL pretraining experiments were conducted on a single NVIDIA GTX 3060 GPU with an Intel i7-6700K CPU. Scale-aware SSL replaces full-resolution views with small-window crops, reducing effective input resolution during pretraining. As a result, SSL pretraining with scale-aware cropping is up to 3x faster than full-image SSL using the same backbone, optimizer, and batch size, while also reducing memory usage and requiring no architectural changes.

4.2. Results and analysis

We showcase our results across both domains in Tables 1 and 2, where the best performing setup for each dataset is highlighted in green. In both cases, the left-hand side of the tables contains results for the full-slice baselines (including the multi-crop VICRegL [22]) and the right-hand side contains our patch-based experiments.

Metric interpretation. Dice score measures pixel-level overlap between prediction and ground truth, emphasizing volumetric accuracy, while Hausdorff distance highlights boundary alignment and structural fidelity. Reporting both allows us to capture not only whether objects are segmented at all, but also whether their geometry is reconstructed correctly.

Small-structure segmentation. We observe that scale-aware SSL with smaller patch sizes consistently improves performance when the targets are small or sparse. For seismic fault segmentation (Table 1, first and second row), Dice scores increase by up to 10%

Table 1: Experiments across seismic datasets

Dataset	Full-slice Baselines						SSL Patch Methods	Patch size L/2		Patch size L/4		Patch size L/8		
	Supervised		SSL		VICRegL			HD	Dice	HD	Dice	HD	Dice	
	HD	Dice	HD	Dice	HD	Dice		HD	Dice	HD	Dice	HD	Dice	
CRACKS	95.51	0.600	88.42	0.591	61.69	0.615	Random Distance	14.27	0.619	11.92	0.615	10.35	0.625	
	110.39	0.513	200	0.491	36.08	0.507		14.51	0.615	14.09	0.601	10.15	0.631	
Thebe	110.39	0.513	200	0.491	36.08	0.507	Random Distance	62.95	0.517	14.32	0.582	13.46	0.612	
	110.39	0.513	200	0.491	36.08	0.507		33.71	0.548	20.15	0.563	13.75	0.591	
CRACKS (facies)	0.027	0.793	0.029	0.792	0.18	0.662	Random Distance	0.019	0.871	0.178	0.763	0.618	0.702	
								0.029	0.863	0.086	0.802	0.821	0.694	

Table 2: Experiments across neuroimaging data

Neural Segmentation Target	Full-slice Baselines						SSL Patch Methods	Patch size L/2		Patch size L/4		Patch size L/8		
	Supervised		SSL		VICRegL			HD	Dice	HD	Dice	HD	Dice	
	HD	Dice	HD	Dice	HD	Dice		HD	Dice	HD	Dice	HD	Dice	
Cells&Vessels (small)	1.85	0.686	1.78	0.685	48.99	0.340	Random Distance	1.16	0.736	1.13	0.731	1.16	0.733	
	1.85	0.686	1.78	0.685	48.99	0.340		1.18	0.736	1.18	0.734	1.30	0.725	
Axons (large)	41.25	0.805	43.02	0.803	29.84	0.589	Random Distance	25.06	0.809	23.30	0.800	24.39	0.790	
	41.25	0.805	43.02	0.803	29.84	0.589		20.83	0.817	24.52	0.814	23.27	0.796	

compared to global-view SSL, with corresponding reductions in Hausdorff distance. For cell and vessel segmentation in neuroimaging, Dice scores improve by up to 5% over the supervised baseline. It is also worth noting that the Hausdorff distance decreases most drastically in the seismic experiments, indicating a much better structural alignment of the detected faults (as showcased visually in Figure 2). Furthermore, in these tasks the smallest patches ($L/8$) yield the strongest gains, confirming that aggressively zooming in on local regions provides the best inductive bias for thin or compact structures. Importantly, our approach outperforms multi-crop VICRegL (a state-of-the-art method designed explicitly for segmentation) particularly in the small-structure experiments, demonstrating that direct scale-aware cropping is a stronger bias than generic multi-crop augmentations.

Large-structure segmentation. In contrast, the same representations do not yield significant improvements for larger structures, as seen in the bottom rows of Tables 1 and 2. For facies segmentation in seismic volumes and axon segmentation in neuroimaging, smaller patches provide little to no benefit, and performance consistently degrades as patch size decreases. In these cases, the largest patches ($L/2$) still provide modest improvements over the full-slice baselines, since segmenting large continuous regions requires retaining broader contextual cues that are discarded when sampling very small windows. This discrepancy underscores that the effectiveness of scale-aware SSL depends critically on the spatial footprint of the target.

Qualitative analysis. Figure 2 further illustrates these trends. While multi-crop VICRegL (Figure 2c) captures more granular structures than vanilla SSL methods, it still fails to reproduce many of the fine-scale discontinuities in faults or the detailed boundaries of cells. By contrast, our patch-based strategy (Figure 2d) recovers significantly more local structure, yielding boundaries that align closely with the ground truth. This qualitative gap reinforces the quantitative improvements observed in Dice and Hausdorff scores.

Taken together, results consistently reveal that SSL representations are not universally effective: their utility depends critically on the spatial footprint of the target. This scale-dependence emerges as a governing factor that determines whether SSL pretraining provides benefits or fails to transfer. Our proposed scale-aware cropping strat-

egy acts as a strong inductive bias for small, sparse structures but can hinder performance on larger, homogeneous ones. This is because smaller crops emphasize localized discontinuities and fine-scale patterns essential for thin or compact objects, but overlook global context that is critical for segmenting extended regions.

5. CONCLUSION

To overcome the inductive biases traditional SSL methods have toward large or dominant structures, we introduce a scale-aware SSL strategy that embeds small-window cropping into the augmentation process, enabling encoders to better capture fine-grained structures during pretraining. Across seismic and neuroimaging domains, our experiments consistently show that this approach yields substantial gains for segmenting small or sparse targets such as faults and cells, while offering limited or even negative benefit for larger structures such as facies and axons. These findings reveal that the effectiveness of SSL is fundamentally scale-dependent: the utility of learned representations is governed by the spatial footprint of the target objects. Rather than being a universal recipe, SSL must be aligned with the geometry of the downstream task. This principle motivates future research into adaptive multi-scale strategies that can reconcile both small and large regimes, ensuring that SSL pipelines remain effective across the full spectrum of scientific imaging tasks.

6. REFERENCES

- [1] Ting Chen, Simon Kornblith, Mohammad Norouzi, and Geoffrey Hinton, “A simple framework for contrastive learning of visual representations,” in *International conference on machine learning*. PMLR, 2020, pp. 1597–1607.
- [2] Kaiming He, Haoqi Fan, Yuxin Wu, Saining Xie, and Ross Girshick, “Momentum contrast for unsupervised visual representation learning,” in *Proceedings of the IEEE/CVF conference on computer vision and pattern recognition*, 2020, pp. 9729–9738.
- [3] Chun-Hsiao Yeh, Cheng-Yao Hong, Yen-Chi Hsu, Tyng-Luh Liu, Yubei Chen, and Yann LeCun, “Decoupled con-

trastive learning,” in *European conference on computer vision*. Springer, 2022, pp. 668–684.

[4] Xinlei Chen and Kaiming He, “Exploring simple siamese representation learning,” in *Proceedings of the IEEE/CVF conference on computer vision and pattern recognition*, 2021, pp. 15750–15758.

[5] Jorge Quesada, Lakshmi Sathidevi, Ran Liu, Nauman Ahad, Joy Jackson, Mehdi Azabou, Jingyun Xiao, Christopher Lidling, Matthew Jin, Carolina Urzay, et al., “Mtneuro: A benchmark for evaluating representations of brain structure across multiple levels of abstraction,” *Advances in neural information processing systems*, vol. 35, pp. 5299–5314, 2022.

[6] Haofeng Li, Yiming Ouyang, and Xiang Wan, “Self-supervised alignment learning for medical image segmentation,” in *2024 IEEE International Symposium on Biomedical Imaging (ISBI)*. IEEE, 2024, pp. 1–5.

[7] Yi Wang, Conrad M Albrecht, Nassim Ait Ali Braham, Lichao Mou, and Xiao Xiang Zhu, “Self-supervised learning in remote sensing: A review,” *IEEE Geoscience and Remote Sensing Magazine*, vol. 10, no. 4, pp. 213–247, 2022.

[8] Dilxat Muhtar, Xueliang Zhang, Pengfeng Xiao, Zhenshi Li, and Feng Gu, “Cmid: A unified self-supervised learning framework for remote sensing image understanding,” *IEEE Transactions on Geoscience and Remote Sensing*, vol. 61, pp. 1–17, 2023.

[9] Alexander Kirillov, Eric Mintun, Nikhila Ravi, Hanzi Mao, Chloe Rolland, Laura Gustafson, Tete Xiao, Spencer Whitehead, Alexander C Berg, Wan-Yen Lo, et al., “Segment anything,” in *Proceedings of the IEEE/CVF International Conference on Computer Vision*, 2023, pp. 4015–4026.

[10] Jorge Quesada, Mohammad Alotaibi, Mohit Prabhushankar, and Ghassan AlRegib, “Pointprompt: A multi-modal prompting dataset for segment anything model,” in *Proceedings of the IEEE/CVF Conference on Computer Vision and Pattern Recognition (CVPR) Workshops*, June 2024, pp. 1604–1610.

[11] Jorge Quesada, Zoe Fowler, Mohammad Alotaibi, Mohit Prabhushankar, and Ghassan AlRegib, “Benchmarking human and automated prompting in the segment anything model,” in *2024 IEEE International Conference on Big Data (BigData)*. IEEE, 2024, pp. 1625–1634.

[12] Jacob Devlin, Ming-Wei Chang, Kenton Lee, and Kristina Toutanova, “Bert: Pre-training of deep bidirectional transformers for language understanding,” in *Proceedings of the 2019 conference of the North American chapter of the association for computational linguistics: human language technologies, volume 1 (long and short papers)*, 2019, pp. 4171–4186.

[13] Mathilde Caron, Hugo Touvron, Ishan Misra, Hervé Jégou, Julien Mairal, Piotr Bojanowski, and Armand Joulin, “Emerging properties in self-supervised vision transformers,” in *Proceedings of the IEEE/CVF international conference on computer vision*, 2021, pp. 9650–9660.

[14] Md. Eshmam Rayed, S.M. Sajibul Islam, Sadia Islam Niha, Jamin Rahman Jim, Md Mohsin Kabir, and M.F. Mridha, “Deep learning for medical image segmentation: State-of-the-art advancements and challenges,” *Informatics in Medicine Unlocked*, vol. 47, pp. 101504, 2024.

[15] Yazeed Alaudah, Patrycja Michałowicz, Motaz Alfarraj, and Ghassan AlRegib, “A machine-learning benchmark for facies classification,” *Interpretation*, vol. 7, no. 3, pp. SE175–SE187, 2019.

[16] Mohit Prabhushankar, Kiran Kokilepersaud, Jorge Quesada, Yavuz Yarici, Chen Zhou, Mohammad Alotaibi, Ghassan AlRegib, Ahmad Mustafa, and Yusufjon Kumakov, “Cracks: Crowdsourcing resources for analysis and categorization of key subsurface faults,” *arXiv preprint arXiv:2408.11185*, 2024.

[17] Jorge Quesada, Chen Zhou, Prithwijit Chowdhury, Mohammad Alotaibi, Ahmad Mustafa, Yusufjon Kumamnov, Mohit Prabhushankar, and Ghassan AlRegib, “A large-scale benchmark on geological fault delineation models: Domain shift, training dynamics, generalizability, evaluation and inferential behavior,” *arXiv preprint arXiv:2505.08585*, 2025.

[18] Sanaz Karimijafarbigloo, Reza Azad, Amirhossein Kazerouni, Yury Velichko, Ulas Bagci, and Dorit Merhof, “Self-supervised Semantic Segmentation: Consistency over Transformation,” Aug. 2023, arXiv:2309.00143 [cs].

[19] Yue Liu, Jun Zeng, Xingzhen Tao, and Gang Fang, “Rethinking Self-Supervised Semantic Segmentation: Achieving End-to-End Segmentation,” *IEEE Transactions on Pattern Analysis and Machine Intelligence*, vol. 46, no. 12, pp. 10036–10046, Dec. 2024.

[20] Jean-Bastien Grill, Florian Strub, Florent Altché, Corentin Tallec, Pierre Richemond, Elena Buchatskaya, Carl Doersch, Bernardo Avila Pires, Zhaohan Guo, Mohammad Gheshlaghi Azar, et al., “Bootstrap your own latent-a new approach to self-supervised learning,” *Advances in neural information processing systems*, vol. 33, pp. 21271–21284, 2020.

[21] Thangarajah Akilan, Nusrat Jahan, and Wandong Zhang, “Self-supervised learning for image segmentation: A comprehensive survey,” *arXiv preprint arXiv:2505.13584*, 2025.

[22] Adrien Bardes, Jean Ponce, and Yann LeCun, “Vicregl: Self-supervised learning of local visual features,” *Advances in Neural Information Processing Systems*, vol. 35, pp. 8799–8810, 2022.

[23] Adrien Bardes, Jean Ponce, and Yann LeCun, “Vicreg: Variance-invariance-covariance regularization for self-supervised learning,” *arXiv preprint arXiv:2105.04906*, 2021.

[24] Yu An, Jiulin Guo, Qing Ye, Conrad Childs, John Walsh, and Ruihai Dong, “A gigabyte interpreted seismic dataset for automatic fault recognition,” *Data in Brief*, vol. 37, pp. 107219, 2021.